Rapid Communications

Nonlocal Coulomb correlations in pure and electron-doped Sr_2IrO_4: Spectral functions, Fermi surface, and pseudo-gap-like spectral weight distributions from oriented cluster dynamical mean-field theory

Cyril Martins,[1] Benjamin Lenz,[2] Luca Perfetti,[3] Veronique Brouet,[4] François Bertran,[5] and Silke Biermann[2,6,*]

[1]*Laboratoire de Chimie et Physique Quantiques, UMR 5626, Université Paul Sabatier, 118 Route de Narbonne, 31400 Toulouse, France*

[2]*Centre de Physique Théorique, Ecole Polytechnique, CNRS UMR 7644, Université Paris-Saclay, Route de Saclay, 91128 Palaiseau, France*

[3]*Laboratoire des Solides Irradiés, Ecole Polytechnique, CNRS, CEA, Université Paris-Saclay, 91128 Palaiseau, France*

[4]*Laboratoire de Physique des Solides, Université Paris-Sud, Université Paris-Saclay, 91405 Orsay, France*

[5]*Synchrotron SOLEIL, L'Orme des Merisiers, Saint-Aubin-BP 48, 91192 Gif sur Yvette, France*

[6]*Collège de France, 11 Place Marcelin Berthelot, 75005 Paris, France*

(Received 22 December 2017; published 12 March 2018)

We address the role of nonlocal Coulomb correlations and short-range magnetic fluctuations in the high-temperature phase of Sr_2IrO_4 within state-of-the-art spectroscopic and first-principles theoretical methods. Introducing an "oriented-cluster dynamical mean-field scheme", we compute momentum-resolved spectral functions, which we find to be in excellent agreement with angle-resolved photoemission spectra. We show that while short-range antiferromagnetic fluctuations are crucial to accounting for the electronic properties of Sr_2IrO_4 even in the high-temperature paramagnetic phase, long-range magnetic order is not a necessary ingredient of the insulating state. Upon doping, an exotic metallic state is generated, exhibiting cuprate-like pseudo-gap spectral properties, for which we propose a surprisingly simple theoretical mechanism.

DOI: 10.1103/PhysRevMaterials.2.032001

Introduction. Sr_2IrO_4 is isostructural to the celebrated high-temperature superconducting copper oxides of the La_2CuO_4 family, but there are even more intriguing similarities in their low energy electronic structure, which is dominated by a single orbital. In the case of cuprates it is a single half-filled x^2-y^2 orbital, subject to strong electronic Coulomb correlations, that determines the low-energy properties, presumably including superconductivity [1]. In the t_{2g}^5 system Sr_2IrO_4, a complex spin-orbit entangled compound orbital carries a single hole [2,3]. While in the cuprates the single-orbital nature of the low-energy electronic structure results from the single-particle band structure, in the iridate it is the result of the joined action of Coulomb interactions and spin-orbit interactions which effectively suppress the degeneracy [4,5].

As in the cuprates, stoichiometric samples of Sr_2IrO_4 are insulating as a result of Coulomb interaction effects, and at low temperatures antiferromagnetic order sets in [6]. The phase diagram has been explored extensively both theoretically [4,5,7–18] and experimentally [2,3,17,19–47]. Sr_2IrO_4 has a strongly temperature-dependent gap that is, however, not affected by the onset of magnetic order. This is *a fortiori* intriguing since even in the paramagnetic phase, long-range two-dimensional antiferromagnetic fluctuations exist, which have been found to exceed 100 lattice spacings [44]. Magnetic exchange interactions seem to be of correspondingly long-range nature [48]. First-principles dynamical mean-field theory (DMFT) calculations [4] can rationalize the insulating nature of the compound, even in its paramagnetic phase. This is consistent with the experimentally found insensitivity of spectral or transport properties on the presence or absence of magnetic order [28,49,50]. Nevertheless the detailed analysis of band dispersions obtained within single-site DMFT reveals interesting discrepancies between theory and experiment (see below). Similar considerations apply to Ba_2IrO_4 [51–53].

Following the analogy with the cuprates, one of the most intriguing questions is the evolution of the electronic structure upon doping. Most interestingly, however, despite all the analogies with the cuprates, to date no superconducting phase has been observed.

A metallic state can be realized via cationic substitution both by hole doping, e.g., with K [36], Rh [49,54,55], or Ru [56], and by electron doping with La [36,50,54,57,58]. For La doping $x \geqslant 0.04$ the system $(Sr_{1-x}La_x)_2IrO_4$ remains a paramagnetic metal down to lowest temperatures [36]. Other possibilities of electron doping are depositing a K surface layer [26,34] and via oxygen depletion [59].

Angle-resolved photoemission spectroscopy (ARPES) has been able to identify the band dispersions and Fermi surfaces in electron- [28,29,32,34,60] and hole-doped [28,32,33] samples. On the electron-doped side, the dominant Fermi surface (FS) feature is a lens-shaped electron pocket centered around M of the crystallographic Brillouin zone (BZ). A detailed analysis of the onset of spectral weight suggests the existence of depletion regions [28,29] reminiscent of the pseudo-gap behavior observed in the cuprates [61–63].

In this paper, we establish a first-principles description of the spectral properties of pure and electron-doped Sr_2IrO_4 beyond the DMFT approximation of a purely local many-body self-energy. We demonstrate that including short-range

*silke.biermann@polytechnique.edu

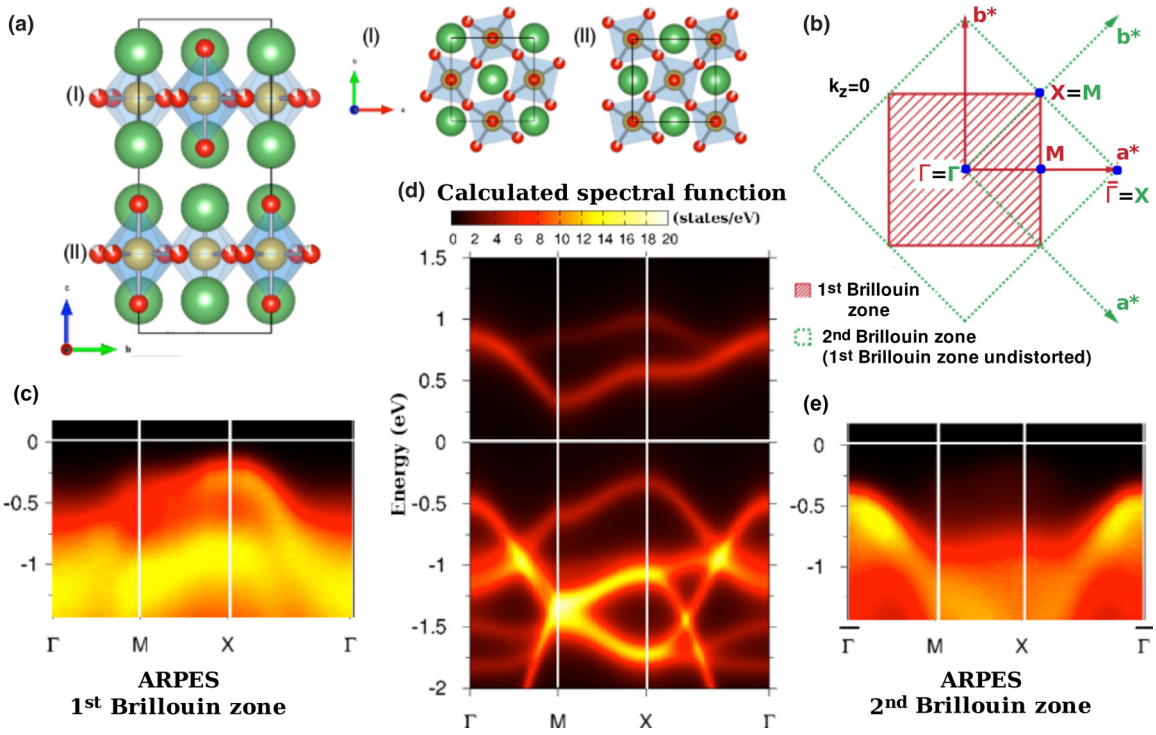

FIG. 1. Spectral function of Sr_2IrO_4. (a) Crystal structure of Sr_2IrO_4. Green spheres stand for Sr, golden ones for Ir, and blue ones for O. The unit cell comprises two layers in the c direction, which are shifted by $(1/2,0)$ in the a-b plane. (b) Illustration of the first BZ of the distorted and undistorted structure of Sr_2IrO_4, and associated high symmetry points. Rotations of the oxygen octahedra cause a doubling of the unit cell, which leads to a halved first BZ. (c) and (e) Measured ARPES spectra in the first and second BZs. (d) Calculated momentum-resolved spectral function of Sr_2IrO_4.

fluctuations is crucial to reliably assessing spectral properties, which we find in excellent agreement with experiments. In the electron-doped case we find an exotic metallic state, which explains recent angle-resolved photoemission spectra. In particular, our calculations offer a surprisingly simple picture for the putative antinodal pseudo-gap found in experiments. It is in fact a direct consequence of strong intersite Ir-Ir fluctuations. Our findings suggest that while the similarities between iridates and cuprates cover various quite different aspects, these common features may not be considered as proxies for superconductivity.

Assessing electronic properties of Sr_2IrO_4. The 5*d* transition metal oxide Sr_2IrO_4 crystallizes into a tetragonal crystal structure derived from the K_2NiF_4 structure, well known in Sr_2RuO_4 or La_2CuO_4, by lowering the symmetry by an 11° rotation of its IrO_6 octahedra around the c axis [52,64,65]. Below 240 K, canted antiferromagnetic order sets in [6,66,67], see Figs. 1(a) and 1(b). Here, we focus on the paramagnetic insulating phase of Sr_2IrO_4 above 240 K.

DMFT-based first-principles calculations that introduce effective Hubbard interactions and assess the resulting quantum fluctuations locally on each Ir atom could indeed identify the insulating state of Sr_2IrO_4 [4,5], even in the absence of long-range magnetic order. The resulting description of spectral properties (see Fig. 3(c) of Ref. [4], which is replotted as Fig. 1 in the Supplemental Material [68]) is, however, not in agreement with experiment.

Here, we introduce an extension of *ab initio* cluster DMFT that extends the concept to *oriented clusters* as representative entities of parts of the solid. As in DMFT, a self-consistency condition restores the original symmetries of the lattice, which—in the case of an oriented cluster—concerns, however, not only the usual translational symmetries, but also the point group of the solid.

Our starting Hamiltonian is the three-orbital Hubbard-type Hamiltonian of Ref. [4], where a single-particle Hamiltonian for the t_{2g} manifold is derived from density functional theory (DFT) calculations and augmented by Hubbard and Hund interaction terms. However, the effect of the interactions onto the $j_{\text{eff}} = 3/2$ states is essentially a global shift that fills these orbitals completely, leaving only the $j_{\text{eff}} = 1/2$ states around the Fermi level [4]. Therefore, we take the result for the $j_{\text{eff}} = 3/2$ states directly from Ref. [4], and include only the $j_{\text{eff}} = 1/2$ states within a tight-binding parametrization into our cluster theory treatment.

The oriented cluster DMFT (OC-DMFT) treatment of this Hamiltonian focuses onto the local Green's function

$$G_{\text{loc}}(\omega) = \sum_{\mathbf{k},\alpha} G_\alpha(\mathbf{k},\omega), \tag{1}$$

with the momentum $\mathbf{k}$- and orientation α-resolved Green's function

$$G_\alpha(\mathbf{k},\omega) = \left[\omega + \mu - H(\mathbf{k}) - \Sigma^\alpha_{\text{dimer}}(\omega)\right]^{-1}. \tag{2}$$

Here, $\Sigma^\alpha_{\text{dimer}}$ is the self-energy of a dimer impurity problem, augmented by an orientation $\alpha = a \pm b$, where a and b are the unit-cell vectors. The $\mathbf{k}$ sum runs over the first BZ

(1BZ), restoring the translational invariance of the solid after calculating its self-energy from the quantum dimer problem, and the sum over α restores its point group. More details on the general philosophy and practical implementation can be found in the Supplemental Material [68].

In a metal, electronic screening is drastically enhanced as compared to an insulator with profound consequences for the spectra [69,70]. This is even more true in 5*d* compounds, where the relatively extended nature of the 5*d* orbitals induces interatomic interactions that are relatively large as compared to the local ones [71]. For this reason, the effective Hubbard interactions are expected to be smaller in the La-doped compound than in the pure sample [72]. We mimic this effect here by using a smaller on-site Hubbard interaction for the doped case ($U_{\text{eff}} = 0.6$ eV) than for the undoped one ($U_{\text{eff}} = 1.1$ eV).

Results for undoped Sr_2IrO_4. We have measured ARPES spectra of Sr_2IrO_4 under the experimental conditions described in the Supplemental Material [68]. Figure 1 displays the resulting spectra along the Γ-M-X-Γ path in the first BZ and the second BZ (2BZ). Due to matrix element effects, these results display characteristic differences, with spectra in the 1BZ amplifying the $j_{\text{eff}} = 1/2$ contribution, while in the 2BZ the $j_{\text{eff}} = 3/2$ contribution is dominant. This strong matrix element effect expresses the fact that the corresponding Fourier component of the potential (lowering the symmetry from $I4/mmm$ to $I4/acd$) is weak. In agreement with ARPES spectra in the literature [28,29], we find the first removal state at Γ to be of $j_{\text{eff}} = 3/2$ character, while the $j_{\text{eff}} = 1/2$ states are strongly dispersive, with a maximum at X. In our theoretical calculations, we do not address matrix element effects, which would differentiate results between different BZs. For this reason, the theoretical spectral function is compared to the sum of the experimental spectra. Most intriguingly, in single-site DMFT calculations (see the Supplemental Material [68]), the $j_{\text{eff}} = 1/2$ states form a very weakly dispersive feature with an onset of spectral weight at -0.2 eV below the Fermi level, in strong disagreement with the experimental spectra in Figs. 1(c) and 1(e).

Figure 1(d) displays the results of our present calculations that include nonlocal many-body correlations within our new OC-DMFT scheme. The comparison to the experimental spectra yields impressive agreement, demonstrating that nonlocal many-body effects were indeed the missing ingredients for assessing spectral properties of this compound. The OC-DMFT treatment effectively includes inter-iridium site fluctuations in the half-filled $j_{\text{eff}} = 1/2$ manifold, and especially includes the intersite magnetic exchange of energy scale $4t^2/U$ into the description. With the present parameters we obtain a value of $\sim$108 meV (78 meV) for states of interlayer (anti)bonding nature, which coincides with the experimental estimate of the magnetic exchange coupling $J = 4t^2/U \sim 100$ meV [44]. As a consequence of the antiferromagnetic fluctuations, the $j_{\text{eff}} = 1/2$ band is much more dispersive than in the single-site DMFT calculation and each of the Hubbard bands [73] has a width of $\sim$0.8 eV.

Our analysis further allows a refinement of the identification of the character of the spectral features. In Fig. 1(c), the signal comes from the 1BZ and is dominated by the $j_{\text{eff}} = 1/2$ manifold, even though along the M-X direction some spectral weight around -1.1 eV originates from the $j_{\text{eff}} = 3/2$ manifold. In Fig. 1(e), the signal comes from the 2BZ and is dominated by the $j_{\text{eff}} = 3/2$ bands. Our calculations show that even within the $j_{\text{eff}} = 3/2$ manifold the experimental signal is selective with respect to the m_j quantum number. The main contribution to the spectral weight seen in the 2BZ comes from the $m_j = 1/2$ band whereas the $m_j = 3/2$ contributes to the 1BZ.

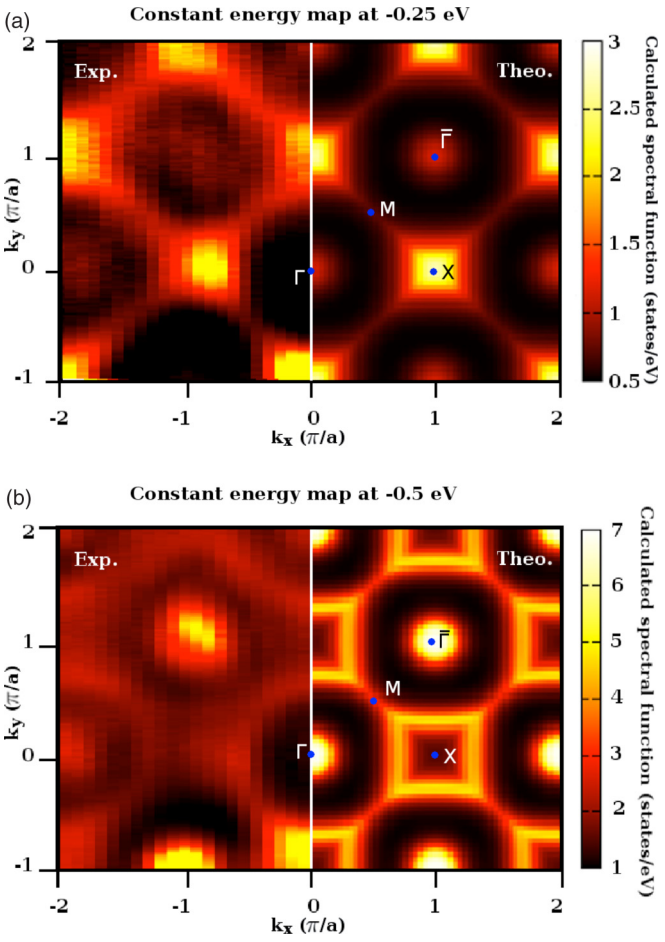

FIG. 2. Constant energy map of the spectral density of Sr_2IrO_4. (a) Experimental (left) and theoretical (right) spectral density at -0.25 eV. (b) The same quantities at -0.5 eV. Blue points indicate high-symmetry points. In the calculations, 1BZ and 2BZ are the same; in the experiments, matrix element effects cause differences.

The left panel of Fig. 2(a) shows an ARPES spectrum acquired at X at -0.25 eV at room temperature. According to ARPES measurements of the magnetic phase, the lowest energy excitations disperse up to the X point and never cross the Fermi level. This spectrum is qualitatively similar to the one measured below T_N in previous works [2,25], demonstrating that spectral properties are largely insensitive to the presence or absence of long-range magnetic order. The lack of a Fermi level crossing excludes the presence of metallic quasiparticles even in the paramagnetic phase, in agreement with theory and experiment. By comparing the measured spectrum with the calculated spectral function, the overall agreement allows a clear identification of the peak at -0.25 eV with the $j_{\text{eff}} = 1/2$ lower Hubbard band (LHB). We show in the left panel of Fig. 2(b) the photoelectron intensity map collected at -0.5 eV. The intense blobs observed at Γ originate from the top level of

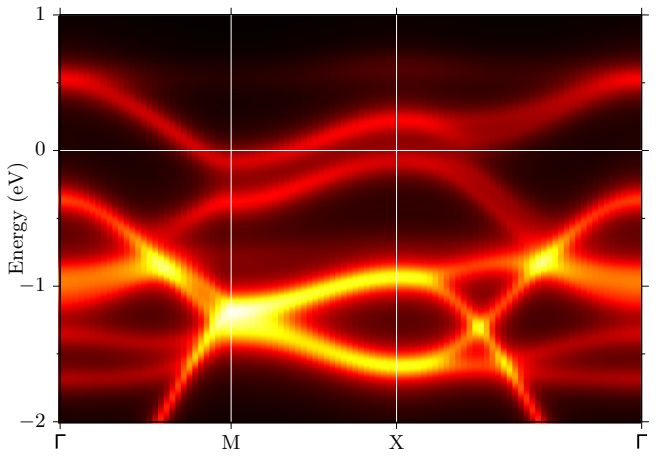

FIG. 3. Calculated momentum-resolved spectral function $A(\mathbf{k},\omega)$ of 10% electron-doped Sr_2IrO_4 along the Γ-M-X-Γ path.

the $j_{\text{eff}} = 3/2$ band, whereas the spectral features around M and X arise from the $j_{\text{eff}} = 1/2$ band and form circles centered around Γ with a radius of 0.5 Å^{-1}.

Results for La*-doped* Sr_2IrO_4 *and the putative pseudo-gap.* In the following, we investigate spectral properties of the electron-doped system and compare our results to experimental findings on $(Sr_{1-x}La_x)_2IrO_4$ with $x = 0.05$ [29]. In this doping regime the system is a paramagnetic metal down to the lowest temperatures.

Figure 3 displays the spectral function $A(\mathbf{k},\omega)$ along the Γ-M-X-Γ path of the BZ resulting from our calculations for an electron doping of 10%. The features of the upper Hubbard band (UHB) of the undoped compound can be continuously connected to features of the quasiparticle states at the Fermi level, which are visible in Fig. 3. In our dimer picture, this reminiscent feature of the UHB arises as bonding and antibonding states of the cluster, which is why we will refer in the following to the lower (upper) branch of the $j_{\text{eff}} = 1/2$ band as the bonding (antibonding) band [73].

The antibonding band (ABB) crosses the Fermi level and causes a Fermi pocket around M. The positions of the band maxima at the high-symmetry points have changed slightly as compared to the undoped case. At M the bonding band (BB) of the $j_{\text{eff}} = 1/2$ appears around -0.37 eV and at X it is in close proximity to the Fermi energy. There, depending on the resolution, spectral weight stemming from the tail of the broad peak can be picked up at the Fermi energy. At Γ the signal of the $j_{\text{eff}} = 3/2$ manifold can be seen at -0.4 eV.

Overall, the spectral function displays excellent agreement with available ARPES data [28,29]. In agreement with Ref. [29] we find a nearly linear dispersion close to the Fermi level, which can be traced back to the ABB. Compared to Ref. [29] our spectrum differs slightly at M in that in Ref. [29] the dispersion close to the Fermi energy was interpreted to extrapolate to a Dirac point around -0.1 eV and a quasilinear continuation for even lower energies, possibly with a small gap at the high-symmetry line. Here, we see a distinct gap between BB and ABB at M and can clearly distinguish between states of the ABB forming the electron pocket and those

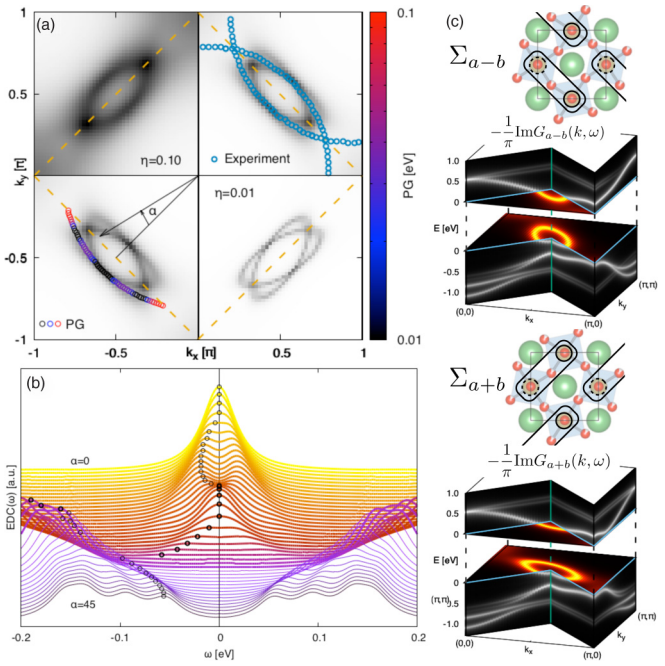

FIG. 4. Spectra of 10%-electron-doped Sr_2IrO_4. (a) Fermi surface. In the first quadrant we overlay experimental data points along which the pseudo-gap was extracted in Ref. [29], and in the third quadrant we overlay the pseudo-gap extracted from the bold lines in (b). (b) Particle-hole averaged ("symmetrized") spectral function for the semicircular $\mathbf{k}$ path used in experimenta [see (a)]. Maxima are indicated by a dot. (c) Calculated spectral function with equal energy cuts at the Fermi surface for Green's functions before orientation average. If not indicated otherwise, the broadening is $\eta = 0.02$ eV.

of the BB. Although the lower part of the experimentally measured dispersion matches our calculated spectrum, the states right below the putative Dirac point are not found here. Our calculation rather suggests a scenario similar to the one of Ref. [28], where a similar quasilinear dispersion was found for a doping of $x = 0.04$. There, the vertical dispersion was discussed as stemming from the spectral weight of the large tail of the $j_{\text{eff}} = 1/2$, which is picked up by the momentum distribution curve [28].

We now turn to the FS. The ABB crosses the Fermi energy close to M resulting in a lens-shaped electron pocket, centered around M [see Fig. 4(a)]. Our theoretical findings agree well with recent ARPES measurements on the electron-doped system $(Sr_{1-x}La_x)_2IrO_4$, considering both the shape and size of the pockets [29].

ARPES also revealed unusual metallic behavior [28,29] with an antinodal pseudo-gap at a La concentration of $x = 0.05$ [29]. Figure 4(b) shows particle-hole averaged spectral functions (symmetrized spectra) as they are often plotted from experimental data. We move along a semicircular k path, which is a natural extension of the Fermi surface [see Fig. 4(a)]. At small angles $4^\circ \leqslant \alpha$ the symmetrized spectral function shows a pseudo-gap, which closes again at $\alpha \approx 15^\circ$. For angles $21^\circ \leqslant \alpha \leqslant 26^\circ$ an additional feature emerges at sufficiently large temperatures, which could be misinterpreted as a pseudo-gap, too. However, since the hole-part of the spectrum is still close to the Fermi energy, this feature can

be traced back to contributions of hole-parts of the spectrum due to large enough temperatures, which then resemble a pseudo-gap in the symmetrized spectra. For angles $\alpha \lesssim 45^\circ$, i.e., close to the antinodal point, spectral features closely resemble the pseudo-gap features emerging at smaller angles close to the tips of the electron pockets. In experiment, based on symmetrized energy distribution curves, the regions outside the pockets were identified as showing a pseudo-gap, which reaches up to the antinodal point [29]. Our calculations reveal that the antinodal regions do not show the same pseudo-gap, which stems from the UHB that forms the pockets, but rather relics of the $j_{\text{eff}} = 1/2$ LHB (Fig. 3). To better understand the origin of pseudo-gap-like features in the symmetrized spectral function, we focus in Fig. 4(a) on FS cuts of the spectral function. Within OC-DMFT we have access to the precise position of the quasiparticle excitations. However, in plots of the spectral function $A(\mathbf{k},\omega)$ we add a finite broadening η to mimic the experimental $\mathbf{k}$ resolution. The top left panel shows the spectral density at the Fermi level with a realistic broadening $\eta = 0.10$ eV. It shows the lens-shaped FS pocket, which is in good agreement with ARPES spectra [29] [top right panel of Fig. 4(a)]. Plotting the extracted pseudo-gap from the symmetrized spectral function in Fig. 4(b) along the semicircular $\mathbf{k}$ path resembles the pseudo-gap found in ARPES (bottom left panel).

We can trace back the origin of the pseudo-gap features by choosing an artificially enhanced resolution [see bottom right panel of Fig. 4(a)], which reveals the fine structure of the Fermi pocket. What seemed to be a sole pocket is actually composed of two separate lens-shaped pockets, which are tilted off-axis in opposite directions by roughly 15° each. Given the experimental resolution, ARPES cannot resolve them separately. The dimer used in our OC-DMFT calculation is the minimal setup to account for the two different IrO_6 orientations of adjacent Ir sites and leads to two configurations (related by a 90° rotation), which are schematically shown in Fig. 4(c). It is the breaking of orientation symmetry within each configuration, which gives rise to the stretched, tilted Fermi pocket at the Fermi energy as shown in the FS cuts of the spectra in Fig. 4(c).

Figure 4(a) shows the FS of the orientation average of both configurations shown in Fig. 4(c). A realistic broadening, however, renders it impossible to identify two separate pockets, but rather suggests an interpretation as a single pocket structure [see Fig. 4(a) for $\eta = 0.10$ eV]. As a consequence, the path along which one extracts the energy distribution curves of this putative single pocket resembles the circular shape of the DFT result that was used in Ref. [29] and does not coincide with the FS of the (two-pocket) FS visible at higher resolution.

Since the putative sole pocket visible at larger broadening is a superposition of the two canted pockets, its tip corresponds to the region between the two pockets. When measuring there, the emerging symmetrized spectral function shown in Fig. 4(b) features a pseudo-gap. In this sense, the appearance of the pseudo-gap close to the pocket's tip is a direct consequence of the nonlocal fluctuations.

Summary and outlook. In conclusion, we have introduced an *ab initio* oriented cluster dynamical mean-field theory which includes nonlocal quantum fluctuations based on an oriented dimer as a reference system for a dynamical mean-field theory scheme. We find excellent agreement between the resulting spectral functions for both pure and electron-doped Sr_2IrO_4 with experimental photoemission data, emphasizing the role of nonlocal quantum correlations in these 5*d* compounds. These findings provide new evidence for the electronic analogies between iridates and cuprates, making the absence of superconductivity an even more intriguing feature of the iridate compounds. In particular, the single-orbital nature of a compound, the emergence of a metallic state from a doped insulating parent compound, and the pseudo-gap-like features discussed for Sr_2IrO_4 do not seem to be proxies for superconductivity.

Acknowledgments. This work was supported by a Consolidator Grant of the European Research Council (Project CorrelMat-617196), the French Agence Nationale de la Recherche under project SOCRATE (Project No. ANR-15-CE30-0009-01) and IDRIS/GENCI Orsay (Project No. t2017091393). We are grateful to the CPHT computer support team.

C.M. and B.L. contributed equally to this work.

[1] B. Keimer, S. A. Kivelson, M. R. Norman, S. Uchida, and J. Zaanen, Nature **518**, 179 (2015).
[2] B. J. Kim, H. Jin, S. J. Moon, J.-Y. Kim, B.-G. Park, C. S. Leem, J. Yu, T. W. Noh, C. Kim, S.-J. Oh, J.-H. Park, V. Durairaj, G. Cao, and E. Rotenberg, Phys. Rev. Lett. **101**, 076402 (2008).
[3] B. J. Kim, H. Ohsumi, T. Komesu, S. Sakai, T. Morita, H. Takagi, and T. Arima, Science **323**, 1329 (2009).
[4] C. Martins, M. Aichhorn, L. Vaugier, and S. Biermann, Phys. Rev. Lett. **107**, 266404 (2011).
[5] C. Martins, M. Aichhorn, and S. Biermann, J. Phys.: Condens. Matter **29**, 263001 (2017).
[6] G. Cao, J. Bolivar, S. McCall, J. E. Crow, and R. P. Guertin, Phys. Rev. B **57**, R11039 (1998).
[7] H. Jin, H. Jeong, T. Ozaki, and J. Yu, Phys. Rev. B **80**, 075112 (2009).
[8] G. Jackeli and G. Khaliullin, Phys. Rev. Lett. **102**, 017205 (2009).
[9] H. Watanabe, T. Shirakawa, and S. Yunoki, Phys. Rev. Lett. **105**, 216410 (2010).
[10] F. Wang and T. Senthil, Phys. Rev. Lett. **106**, 136402 (2011).
[11] B. H. Kim, G. Khaliullin, and B. I. Min, Phys. Rev. Lett. **109**, 167205 (2012).
[12] R. Arita, J. Kunes, A. V. Kozhevnikov, A. G. Eguiluz, and M. Imada, Phys. Rev. Lett. **108**, 086403 (2012).
[13] H. Zhang, K. Haule, and D. Vanderbilt, Phys. Rev. Lett. **111**, 246402 (2013).
[14] Z. Y. Meng, Y. B. Kim, and H.-Y. Kee, Phys. Rev. Lett. **113**, 177003 (2014).
[15] J.-i. Igarashi and T. Nagao, Phys. Rev. B **90**, 064402 (2014).

[16] H. Watanabe, T. Shirakawa, and S. Yunoki, Phys. Rev. B **89**, 165115 (2014).

[17] Y. Liu, L. Yu, X. Jia, J. Zhao, H. Weng, Y. Peng, C. Chen, Z. Xie, D. Mou, J. He, X. Liu, Y. Feng, H. Yi, L. Zhao, G. Liu, S. He, X. Dong, J. Zhang, Z. Xu, C. Chen, G. Cao, X. Dai, Z. Fang, and X. J. Zhou, Sci. Rep. **5**, 13036 (2015).

[18] I. V. Solovyev, V. V. Mazurenko, and A. A. Katanin, Phys. Rev. B **92**, 235109 (2015).

[19] S. J. Moon, H. Jin, K. W. Kim, W. S. Choi, Y. S. Lee, J. Yu, G. Cao, A. Sumi, H. Funakubo, C. Bernhard, and T. W. Noh, Phys. Rev. Lett. **101**, 226402 (2008).

[20] S. J. Moon, H. Jin, W. S. Choi, J. S. Lee, S. S. A. Seo, J. Yu, G. Cao, T. W. Noh, and Y. S. Lee, Phys. Rev. B **80**, 195110 (2009).

[21] D. Hsieh, F. Mahmood, D. H. Torchinsky, G. Cao, and N. Gedik, Phys. Rev. B **86**, 035128 (2012).

[22] L. Zhao, D. H. Torchinsky, H. Chu, V. Ivanov, R. Lifshitz, R. Flint, T. Qi, G. Cao, and D. Hsieh, Nat. Phys. **12**, 32 (2016).

[23] D. Pröpper, A. N. Yaresko, M. Höppner, Y. Matiks, Y.-L. Mathis, T. Takayama, A. Matsumoto, H. Takagi, B. Keimer, and A. V. Boris, Phys. Rev. B **94**, 035158 (2016).

[24] Y. Li, R. D. Schaller, M. Zhu, D. A. Walko, J. Kim, X. Ke, L. Miao, and Z. Q. Mao, Sci. Rep. **6**, 19302 (2016).

[25] Q. Wang, Y. Cao, J. A. Waugh, S. R. Park, T. F. Qi, O. B. Korneta, G. Cao, and D. S. Dessau, Phys. Rev. B **87**, 245109 (2013).

[26] Y. K. Kim, O. Krupin, J. D. Denlinger, A. Bostwick, E. Rotenberg, Q. Zhao, J. F. Mitchell, J. W. Allen, and B. J. Kim, Science **345**, 187 (2014).

[27] A. Yamasaki, S. Tachibana, H. Fujiwara, A. Higashiya, A. Irizawa, O. Kirilmaz, F. Pfaff, P. Scheiderer, J. Gabel, M. Sing, T. Muro, M. Yabashi, K. Tamasaku, H. Sato, H. Namatame, M. Taniguchi, A. Hloskovskyy, H. Yoshida, H. Okabe, M. Isobe, J. Akimitsu, W. Drube, R. Claessen, T. Ishikawa, S. Imada, A. Sekiyama, and S. Suga, Phys. Rev. B **89**, 121111 (2014).

[28] V. Brouet, J. Mansart, L. Perfetti, C. Piovera, I. Vobornik, P. Le Fèvre, F. Bertran, S. C. Riggs, M. C. Shapiro, P. Giraldo-Gallo, and I. R. Fisher, Phys. Rev. B **92**, 081117 (2015).

[29] A. de la Torre, S. M. Walker, F. Y. Bruno, S. Riccó, Z. Wang, I. Gutierrez Lezama, G. Scheerer, G. Giriat, D. Jaccard, C. Berthod, T. K. Kim, M. Hoesch, E. C. Hunter, R. S. Perry, A. Tamai, and F. Baumberger, Phys. Rev. Lett. **115**, 176402 (2015).

[30] Y. F. Nie, P. D. C. King, C. H. Kim, M. Uchida, H. I. Wei, B. D. Faeth, J. P. Ruf, J. P. C. Ruff, L. Xie, X. Pan, C. J. Fennie, D. G. Schlom, and K. M. Shen, Phys. Rev. Lett. **114**, 016401 (2015).

[31] J. K. Kawasaki, M. Uchida, H. Paik, D. G. Schlom, and K. M. Shen, Phys. Rev. B **94**, 121104 (2016).

[32] C. Piovera, V. Brouet, E. Papalazarou, M. Caputo, M. Marsi, A. Taleb-Ibrahimi, B. J. Kim, and L. Perfetti, Phys. Rev. B **93**, 241114 (2016).

[33] Y. Cao, Q. Wang, J. A. Waugh, T. J. Reber, H. Li, X. Zhou, S. Parham, S.-R. Park, N. C. Plumb, E. Rotenberg, A. Bostwick, J. D. Denlinger, T. Qi, M. A. Hermele, G. Cao, and D. S. Dessau, Nat. Commun. **7**, 11367 (2016).

[34] Y. K. Kim, N. H. Sung, J. D. Denlinger, and B. J. Kim, Nat. Phys. **12**, 37 (2016).

[35] S. Chikara, O. Korneta, W. P. Crummett, L. E. DeLong, P. Schlottmann, and G. Cao, Phys. Rev. B **80**, 140407 (2009).

[36] M. Ge, T. F. Qi, O. B. Korneta, D. E. De Long, P. Schlottmann, W. P. Crummett, and G. Cao, Phys. Rev. B **84**, 100402 (2011).

[37] D. A. Zocco, J. J. Hamlin, B. D. White, B. J. Kim, J. R. Jeffries, S. T. Weir, Y. K. Vohra, J. W. Allen, and M. B. Maple, J. Phys.: Condens. Matter **26**, 255603 (2014).

[38] L. Fruchter, G. Collin, D. Colson, and V. Brouet, Eur. Phys. J. B **88**, 141 (2015).

[39] I. Pallecchi, M. T. Buscaglia, V. Buscaglia, E. Gilioli, G. Lamura, F. Telesio, M. Cimberle, and D. Marré, J. Phys.: Condens. Matter **28**, 065601 (2016).

[40] G. Zhou, X. Gu, X. Yang, X. Gao, K. Wang, J. Peng, F. Zhang, and X. S. Wu, AIP Adv. **7**, 055823 (2017).

[41] Q. Li, G. Cao, S. Okamoto, J. Yi, W. Lin, B. C. Sales, J. Yan, R. Arita, J. Kunes, A. V. Kozhevnikov, A. G. Eguiluz, M. Imada, Z. Gai, M. Pan, and D. G. Mandrus, Sci. Rep. **3**, 3073 (2013).

[42] J. Dai, E. Calleja, G. Cao, and K. McElroy, Phys. Rev. B **90**, 041102 (2014).

[43] D. Haskel, G. Fabbris, M. Zhernenkov, P. P. Kong, C. Q. Jin, G. Cao, and M. van Veenendaal, Phys. Rev. Lett. **109**, 027204 (2012).

[44] S. Fujiyama, H. Ohsumi, T. Komesu, J. Matsuno, B. J. Kim, M. Takata, T. Arima, and H. Takagi, Phys. Rev. Lett. **108**, 247212 (2012).

[45] J. Kim, D. Casa, M. H. Upton, T. Gog, Y.-J. Kim, J. F. Mitchell, M. van Veenendaal, M. Daghofer, J. van den Brink, G. Khaliullin, and B. J. Kim, Phys. Rev. Lett. **108**, 177003 (2012).

[46] S. Fujiyama, H. Ohsumi, K. Ohashi, D. Hirai, B. J. Kim, T. Arima, M. Takata, and H. Takagi, Phys. Rev. Lett. **112**, 016405 (2014).

[47] J. Kim, M. Daghofer, A. H. Said, T. Gog, J. van den Brink, G. Khaliullin, and B. J. Kim, Nat. Commun. **5**, 4453 (2014).

[48] S. Agrestini, C.-Y. Kuo, M. M. Sala, Z. Hu, D. Kasinathan, K.-T. Ko, P. Glatzel, M. Rossi, J.-D. Cafun, K. O. Kvashnina, A. Matsumoto, T. Takayama, H. Takagi, L. H. Tjeng, and M. W. Haverkort, Phys. Rev. B **95**, 205123 (2017).

[49] T. F. Qi, O. B. Korneta, L. Li, K. Butrouna, V. S. Cao, X. Wan, P. Schlottmann, R. K. Kaul, and G. Cao, Phys. Rev. B **86**, 125105 (2012).

[50] H. D. Zhao, J. Terzic, H. Zheng, Y. F. Ni, Y. Zhang, F. Ye, P. Schlottmann, and G. Cao, arXiv:1712.05518.

[51] A. Hampel, C. Piefke, and F. Lechermann, Phys. Rev. B **92**, 085141 (2015).

[52] S. Moser, L. Moreschini, A. Ebrahimi, B. D. Piazza, M. Isobe, H. Okabe, J. Akimitsu, V. V. Mazurenko, K. S. Kim, A. Bostwick, E. Rotenberg, J. Chang, H. M. Rønnow, and M. Grioni, New J. Phys. **16**, 013008 (2014).

[53] M. Uchida, Y. F. Nie, P. D. C. King, C. H. Kim, C. J. Fennie, D. G. Schlom, and K. M. Shen, Phys. Rev. B **90**, 075142 (2014).

[54] Y. Klein and I. Terasaki, J. Phys.: Condens. Matter **20**, 295201 (2008).

[55] J. S. Lee, Y. Krockenberger, K. S. Takahashi, M. Kawasaki, and Y. Tokura, Phys. Rev. B **85**, 035101 (2012).

[56] S. Calder, J. W. Kim, G.-X. Cao, C. Cantoni, A. F. May, H. B. Cao, A. A. Aczel, M. Matsuda, Y. Choi, D. Haskel, B. C. Sales, D. Mandrus, M. D. Lumsden, and A. D. Christianson, Phys. Rev. B **92**, 165128 (2015).

[57] X. Chen, T. Hogan, D. Walkup, W. Zhou, M. Pokharel, M. Yao, W. Tian, T. Z. Ward, Y. Zhao, D. Parshall, C. Opeil, J. W. Lynn, V. Madhavan, and S. D. Wilson, Phys. Rev. B **92**, 075125 (2015).

[58] I. Battisti, V. Fedoseev, K. M. Bastiaans, A. de la Torre, R. S. Perry, F. Baumberger, and M. P. Allan, Phys. Rev. B **95**, 235141 (2017).

[59] O. B. Korneta, T. Qi, S. Chikara, S. Parkin, L. E. De Long, P. Schlottmann, and G. Cao, Phys. Rev. B **82**, 115117 (2010).

[60] H. Gretarsson, N. H. Sung, J. Porras, J. Bertinshaw, C. Dietl, J. A. N. Bruin, A. F. Bangura, Y. K. Kim, R. Dinnebier, J. Kim, A. Al-Zein, M. Moretti Sala, M. Krisch, M. Le Tacon, B. Keimer, and B. J. Kim, Phys. Rev. Lett. **117**, 107001 (2016).

[61] H. Alloul, T. Ohno, and P. Mendels, Phys. Rev. Lett. **63**, 1700 (1989).

[62] H. Ding, T. Yokoya, J. C. Campuzano, T. Takahashi, M. Randeria, M. R. Norman, T. Mochiku, K. Kadowaki, and J. Giapintzakis, Nature **382**, 51 (1996).

[63] A. G. Loeser, Z.-X. Shen, D. S. Dessau, D. S. Marshall, C. H. Park, P. Fournier, and A. Kapitulnik, Science **273**, 325 (1996).

[64] Q. Huang, J. L. Soubeyroux, O. Chmaissem, I. Natali Sora, A. Santoro, R. J. Cava, J. J. Krajewski, and W. F. Peck, J. Solid State Chem. **112**, 355 (1994).

[65] Further reduction of the symmetry by staggered tetragonal distortion of the IrO_6 octahedra has not been considered here. See D. H. Torchinsky, H. Chu, L. Zhao, N. B. Perkins, Y. Sizyuk, T. Qi, G. Cao, and D. Hsieh, Phys. Rev. Lett. **114**, 096404 (2015).

[66] R. J. Cava, B. Batlogg, K. Kiyono, H. Takagi, J. J. Krajewski, W. F. Peck, L. W. Rupp, and C. H. Chen, Phys. Rev. B **49**, 11890 (1994).

[67] M. K. Crawford, M. A. Subramanian, R. L. Harlow, J. A. Fernandez-Baca, Z. R. Wang, and D. C. Johnston, Phys. Rev. B **49**, 9198 (1994).

[68] See Supplemental Material at http://link.aps.org/supplemental/10.1103/PhysRevMaterials.2.032001 for experimental details and more details on the general philosophy, practical implementation and technical details of Oriented-Cluster-DMFT.

[69] T. Ayral, S. Biermann, and P. Werner, Phys. Rev. B **87**, 125149 (2013).

[70] T. Ayral, S. Biermann, P. Werner, and L. Boehnke, Phys. Rev. B **95**, 245130 (2017).

[71] H. Jiang *et al.* (unpublished preliminary results).

[72] P. Liu, M. Reticcioli, B. Kim, A. Continenza, G. Kresse, D. D. Sarma, X.-Q. Chen, and C. Franchini, Phys. Rev. B **94**, 195145 (2016)

[73] From the dimer cluster used within our OC-DMFT treatment, four spectral branches emerge: A bonding and antibonding band and two corresponding satellites, see also J. M. Tomczak, Ph.D. thesis, Ecole Polytechnique, 2007. Therefore one should rather refer to the branches with large spectral weight visible in the spectral plot of Fig. 1(d) as (anti)bonding bands. Actually the correlation satellites or Hubbard bands are the outer excitations and carry less spectral weight. However, to be consistent with the notation in standard literature on Sr_2IrO_4 we use the notion of Hubbard bands when discussing the undoped compound.